A CFD assessment of classifications for hypersonic inlet start/unstart phenomena

J. Chang, D. Yu, W. Bao, Z. Xie and Y. Fan
juntao_chang@yahoo.com.cn
Harbin Institute of Technology
Heilongjiang, China

ABSTRACT

Inlet start/unstart detection is one of the most important issues of hypersonic inlets and is also the foundation of protection controls of scramjets. In ground and flight tests, it is inevitably to introduce the sensor noises to the measurement system. How to overcome or weaken the influence of the sensor noises and the outer disturbances is an important issue to the control system of the engine. To solve this problem, the 2D inner steady flow of hypersonic inlets was numerically simulated in different freestream conditions and backpressures, and two different inlet unstart phenomena were analysed. The membership function for hypersonic inlet start/unstart can be obtained by using probabilistic output support vector machine, and the algorithm of multiple classifiers fusion is introduced. The variations of the classification accuracy with the intensity of the sensor noises and the number of the classifier were discussed respectively. In conclusion, it is useful to introduce the algorithm of support vector machine and multiple classifiers fusion to overcome or weaken the influence of the sensor noises on the classification accuracy of hypersonic inlet start/unstart. The number of the practical fusion classifiers needs a tradeoff between the fusion classification accuracy and the complexity of the classification system.

NOMENCLATURE

M_∞	Mach number of the freestream
T_∞	static temperature of the freestream
p_∞	static pressure of the freestream
p_s	surface static pressure of the inlet
x	axis location of the inlet
x_1	shown in Fig. 1, behind of the first oblique shock
x_2	shown in Fig. 1, under the lip
p_1	static pressure at x_1
p_2	static pressure at x_2
p_{min}	mass-weighted average static pressure at entrance of isolator
p_{max}	static pressure larger than the maximal sustainable backpressure of the isolator
p_b	static pressure at the exit of isolator
q	probability density
A	parameter of membership function
B	parameter of membership function
f	output of support vector machine
k	turbulent kinetic energy
y^+	the wall yplus
α	angle-of-attack of the freestream
ε	turbulent dissipation rate

Paper No. 3341. Manuscript received 4 September 2008, revised version received 30 November 2008 accepted 18 December 2008.

1.0 INTRODUCTION

The performance of a ramjet-scramjet powered hypersonic vehicle is determined by its inlet efficiency. Specifically, the inlet wave system influences compression efficiency, mass capture and combustion stability. The unstart phenomenon is one of the most important issues of the hypersonic inlet. The disturbances which can induce inlet unstart can be either the variation of flight conditions (i.e. angle-of-attack, freestream Mach number, freestream pressure, etc.) or the disturbance of the combustor. For hypersonic airbreathing engines, inlet unstart causes a large drop of both engine thrust and specific impulse, thus it may cause catastrophic damage during hypersonic flight. So quick and reliable inlet start/unstart detection is necessary to the control systems of the engine because the loss of engine thrust caused by inlet unstart results in a deceleration of the spaceplane or even a mission failure[1,2]. Furthermore from the viewpoint of the engine control systems, disturbances are introduced into the engine control system by accelerations that are several times larger than those of a transport, when the control system needs overcome the influence of the sensor noise and the outer disturbances for the proper detection of inlet start/unstart. How to overcome or weaken the influence of the sensor noises and the outer disturbances on the classification accuracy of hypersonic inlet start/unstart is an important issue to the control system of the engine.

Unstart phenomena of the hypersonic inlet have been very active fields of research in last decades, there have been many papers devoted to this subject[3-16]. Mayer and Paynter[3,4] used an Euler solver and simulated an axisymmetric inlet unstart due to the variation of freestream variables such as temperature, velocity and pressure. Neaves and McRae[5] developed dynamic solution-adaptive gird algorithm introduced by Benson and McRae[6] and simulated the 3D inlet unstart caused by a combustor perturbation. Zha[7,8] investigated unstart transient mechanism of a typical axisymmetric HSCT (High Speed Civil Transport) inlet at angle of attack using CFD. C. Cox[9] presented several mechanisms of hypersonic inlet unstart, including backpressure unstart, overcontraction unstart, and angle of attack unstart. Chang[10] investigated the dimensionless analysis of unstart boundary of the hypersonic inlet by means of the dimensional analysis. Schmitz[11] and Van Wie[12] analysed the major factors that influence the inlet operation mode and studied the start/unstart characteristic of the 2D hypersonic inlet. Reinartz[13] and Saied Emami[14] studied the variation of isolator geometry and its influence on the overall inlet compression efficiency. The detection[15] has been proposed and several measurement techniques provided useful information by which to evaluate the inlet operating mode that is the flow visualization technique using the shadowgraph/Schlieren windows, and the visualization technique is complex and not practical to the flight test. Yu[16] discussed the optimal classification criterions of the hypersonic inlet start/unstart based on 'numerical experimental' data by the support vector machine-recursive feature elimination algorithm and Fisher linear discriminant analysis.

However, few numerical and experimental investigations have been reported on weakening or overcoming the effect of the measurement noises or the larger disturbances on the classification accuracy of hypersonic inlet start/unstart. In the flight test[17], the engine control system determines the inlet start/unstart by a ratio of the pressure near the entrance of isolator to the pressure under the lip. Unfortunately, the inlet operation mode is not properly sensed, which results in the part failure of flight test. The possible reason why the control system could not properly sense inlet start and inlet unstart is the improper classification criterion or the influence of the sensor noise and the outer disturbances which cause the false detection.

Learning pattern classification has been developed in the past decades[18]. Pattern classification is the act of taking in the raw data and taking an action based on the 'category' of the pattern. SVM (support vector machine) is as a powerful pattern classification tool for solving classification problems[16]16, but there are still some limitations of this theory. In many real-world applications, the importance of the training points is different. It is often that some training points are more important than others in the classification problem. We would require that the meaningful training points must be classified correctly and would not care about some training points like noises whether or not they are misclassified. That is, each training point no more exactly belongs to one of the two classes. It may 90% belong to one class and 10% be meaningless, and it may 20% belong to one class and 80% be meaningless. In other words, there is a fuzzy membership associated with each training point. This fuzzy membership can be regarded as the attitude of the corresponding training point toward one class in the classification problem. This is the basic idea of the fuzzy. FSVM (fuzzy SVM) is the combination of the concept of SVM with the fuzzy membership.

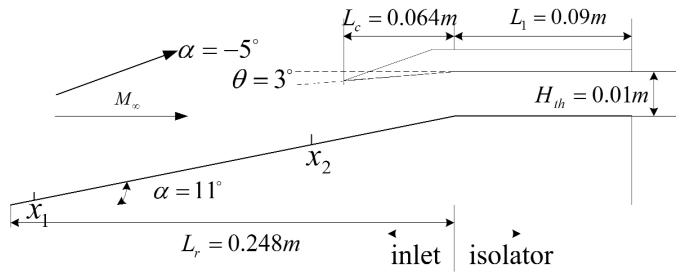

Figure 1. Geometric sketch of the inlet model.

In this paper, the study is focused on the MCF (multiple classifiers fusion) method to improve the classification reliability of hypersonic inlet start/unstart based on the simulation results. The inlet unstart phenomena (back pressure unstart, low Mach number unstart) were studied firstly. Based on the 'numerical experiment' data, the POSVM (probabilistic output SVM) by which the membership function is obtained and MCF by which the effect of the sensor noises on the classification accuracy is weakened are introduced to improve the classification accuracy of hypersonic inlet start/unstart with the sensor noises and outer disturbances. The rest of this paper is organised as follows. Section 2 states data preparation for pattern classification of hypersonic inlet start/unstart. Section 3 presents the classification of hypersonic inlet start/unstart by using POSVM. The MCF of hypersonic inlet start/unstart is given in Section 4. Section 5 presents some conclusions.

2.0 DATA PREPARATION FOR PATTERN CLASSIFICATION OF HYPERSONIC INLET START/UNSTART

Pattern classification is the act of taking in the raw data and taking an action based on the 'category' of the pattern. For the pattern classification of hypersonic inlet start/unstart, the first step is to obtain the surface pressure distributions which include the inlet start and inlet unstart. The data can be acquired by the numerical simulation or experiment of the hypersonic inlet.

2.1 Inlet model and numerical method

The overall inlet geometry is based on the similar inlet model tested within the frame of earlier Langley Research Center activities[14]. The inlet model mentioned above is simplified in computation because the principal aim of this paper is to research the pattern classification of inlet start/unstart. The computational model includes an inlet and constant area isolator only. Figure 1 shows the geometric sketch of the inlet model.

https://doi.org/10.1017/S0001924000002931 Published online by Cambridge University Press

Table 1
Boundary conditions for Case I, II and III

Case	M_∞	T_∞/K	p_∞/p_a	p_b/p_a	Angle-of-attack α,deg
I	4	216·6	8,471	$[p_{min}, p_{max}]$	–10 ,-5, 0, 5, 10
II	5	216·7	5,415	$[p_{min}, p_{max}]$	–10 ,–5, 0, 5, 10
III	6	219·1	3,743	$[p_{min}, p_{max}]$	–10 ,–5, 0, 5, 10

Table 2
Performance parameter of hypersonic inlets at different grid-refinement levels

Grid level	ϕ	σ	p_3/p_0
Coarse	0·711	0·341	13·12
Medium	0·705	0·352	13·05
Fine	0·722	0·358	13·25

The computation is performed using the finite-volume technique with upwind discretisation to solve the two-dimensional compressible Reynolds-averaged Navier-Stokes equations[19]. The space discretisation is performed by a cell-centered formulation. To account for the directed propagation of information in the inviscid part of the equations, the advection upstream splitting method (AUSM) flux vector splitting is applied for the approximation of the convective flux functions. Higher-order accuracy for the upwind discretiszation and consistency with the central differences used for the diffusive term is achieved by the monotonic upstream scheme for conservation laws extrapolations, and the total variation diminishing property of the scheme is ensured by the Van Leer flux limiter. To enhance convergence, a multigrid method, implicit residuals smoothing, and local time stepping are applied. To ensure the accuracy of the turbulence flow solution, a value of y^+ below 5 is realized for the main portion of the wall flow region. To simulate the interaction between the shock and the boundary layer, the intersection, and reflection of wave system, calculate the flow field at first, and perform the mesh self-adaptation technology based on the pressure gradient and continue to compute.

A Renormalisation Group k-ε turbulence model is implemented for turbulent flows. The boundary condition of the supersonic inflow is far-pressure field, and the freestream conditions given in Table 1 can be defined by specifying the boundary conditions, where the definition of α is referred to Fig. 1. The boundary condition of the exit of the isolator is the pressure outlet, and the backpressure can be defined by specifying the pressure value. In case of predominant supersonic outflow, the variables are completely extrapolated from the interior to the boundary. Otherwise, the influence of the throttle is simulated with a prescribed backpressure at the outflow boundary and the remaining variables are extrapolated. At solid walls, the no-slip boundary condition is enforced by setting the velocity components to zero.

2.2 Numerical accuracy analysis

To ensure the convergence of the numerical solution, the residuals (L_2-norm) are monitored in Fig. 2. The solution can be considered as converged after approximately 75,000 iterations, where the courant number is 0·5. At this stage, the continuity residual, x-velocity residual, y-velocity residual and energy residual reach their minimum values after falling for over four orders of magnitude. The turbulence (k and ε) residual have a six orders of magnitude decrease. An additional convergence criterion enforced in this current analysis requires the difference between computed inflow and outflow mass flux to drop below 0·5%.

The performance of a grid sensitivity analysis confirmed that the grid resolution used here is sufficient. Table 2 shows the performance parameters (mass-captured coefficient, total-pressure recovery coefficient and static pressure ratio) of hypersonic inlets

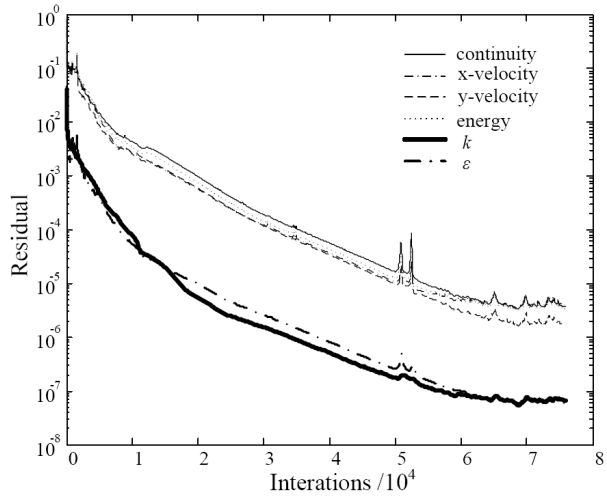

Figure 2. Residuals for hypersonic inlet computations.

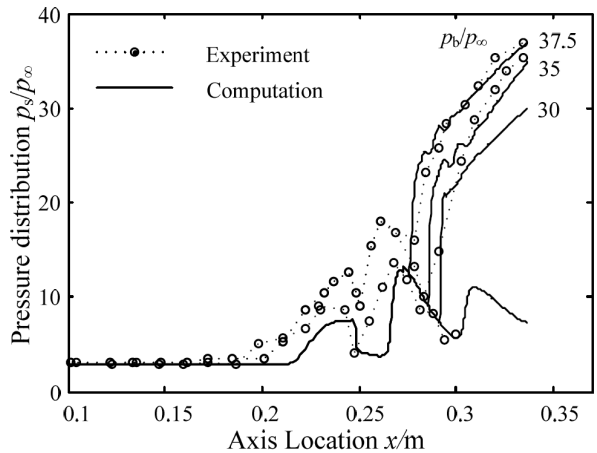

Figure 3. Surface pressure distributions with different backpressures, $M_\infty = 4$ and $\alpha = 0$.

($M_0 = 6$, $p_0 = 3{,}743p_a$, $T_0 = 219{\cdot}1$K) at different grid-refinement levels: coarse (740 × 60), medium (910 × 110), and fine (1,610 × 190); and the maximum discrepancy between the three mesh levels is less than 3%, where the performance parameter is referred to the one (mass-weighted averaged) at the exit of the isolator. Out of this analysis, the medium grid was selected, and all results shown are computed applying this resolution. The use of a medium grid resolution greatly saves the CPU time.

The accuracy of the current numerical investigation is evaluated by comparison with the experimental results. The experimental data is referred to Fig. 7 and Fig. 19(e) in Ref. 14. The surface pressure distributions are shown in Fig. 3. Comparison of a Schlieren picture[13,20] without throttling and corresponding Mach number contour lines of the computation is shown in Fig. 4, and it reveals an overall good agreement. The shock wave pattern, the separation, and the approximate boundary-layer thickness of the Schlieren picture are also present in the simulation results. The surface pressure distributions shown in Fig. 5, allow for a more quantitative comparison between numerical and experimental results. Here, a discrepancy in the ramp pressure distribution can be seen in the expansion region

https://doi.org/10.1017/S0001924000002931 Published online by Cambridge University Press

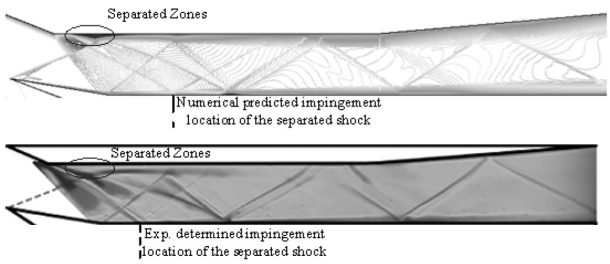

Figure 4. Comparison of a Schlieren picture (bottom) without throttling and corresponding Mach number contour lines (top) of the computation.

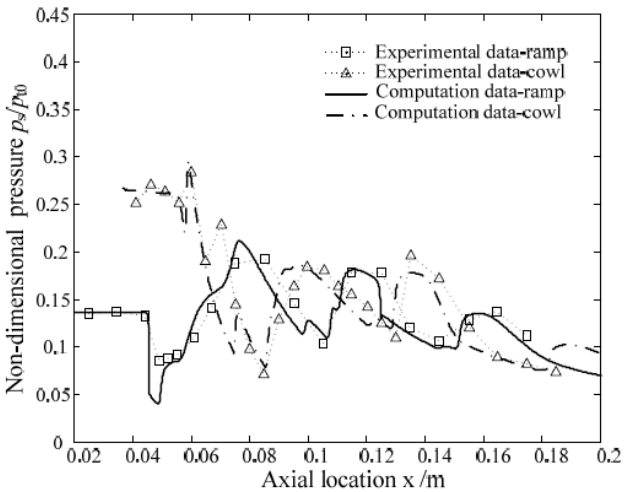

Figure 5. Surface pressure distributions of hypersonic inlets.

with subsequent separation. The computed separation appears smaller than experimentally observed, and thus, the separation shock is weaker and impinges downstream of the measured location on the cowl surface. The reason for the discrepancy is probably the deficiency of the turbulence model, the differences between experiment and computation conditions, or the measurements error of the sensor. In a word, the computation results of the hypersonic inlet accord with the physical conception of the aerodynamics. It can reveal the intersection of oblique shock waves and expansion waves and capture the primary characteristic of internal flowfield. The simulation results can be used as data to investigate the multiple classifiers fusion of hypersonic inlet start/unstart.

2.3 Inlet unstart data composition and analysis

Generally speaking, there are two main different classes of inlet unstart for the fixed geometry hypersonic inlet, one is backpressure unstart, and the other is low Mach number unstart. The unstart data set includes the two classes of inlet surface pressure distributions.

In scramjet, a precombustion shock system is developed inside of the isolator because of the subsequent high-pressure combustion zone. To produce a similar shock wave system in the test, the effect of the operating engine is simulated by a specified backpressure. Fig. 3 shows surface pressure distributions with different backpressure ratios. The high backpressure leads to the separation of the boundary layer. The pressure buildup proceeds continuously due to the rapidly growing boundary layer. As the backpressure increases, the onset of pressure buildup moves upstream into the isolator. At p_b/p_∞ = 37·5,

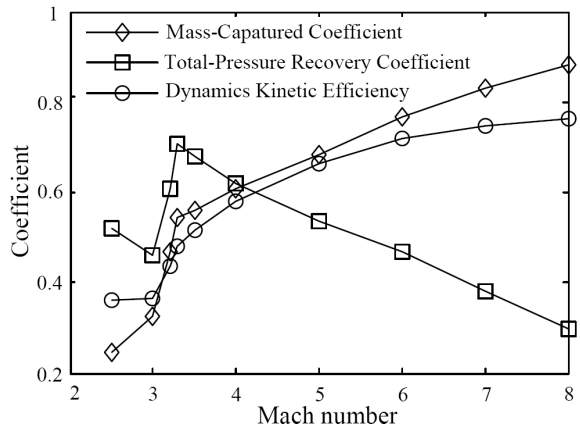

Figure 6. Variations of mass-captured coefficient, total pressure recovery coefficient and dynamics kinetic efficiency with the Mach number of freestream.

the complete isolator contributes to the pressure buildup, and the maximum pressure ratio p_b/p_∞ is achieved. After even a slight shift of the operating point (p_b/p_∞ = 37·5), the pressure rise is pushed forward into the contracting part of the inlet. A further increase of the backpressure causes a severe flow blockage and results in a strong decrease of the captured mass flow. In this condition, the inlet flowfield is unstable and the inlet is no longer started.

The internal contraction ration of hypersonic inlet is about 1·9, which is above the Kantrowitz limit for self starting. Figure 6 shows the variations of mass-captured coefficient, total-pressure recovery coefficient and kinetic energy efficiency with the Mach number of freestream, where the performance index is referred to the one (mass-weighted averaged) at the exit of the isolator. As Mach number of freestream decreases, the mass-captured coefficient and kinetic energy efficiency gradually decreases and the total-pressure recovery coefficient increases. When Mach number decreases to Mach 3·2, the performance parameter varies abruptly because the separated flow appears and the backward shock is formed; thus the inlet is no longer started. The starting Mach number of the hypersonic inlet is about 3·2 at the attack-of-angle zero. Here the term 'started' is used to denote the operation mode under which the shock system structures in the internal portions of the inlet do not alter the mass-captured characteristics. This is the essence difference between inlet start and unstart. However you approach the CFD solutions, the inlet start or unstart can be defined based on the mass-captured characteristics.

The numerical accuracy analysis of the hypersonic inlet unstart phenomena (backpressure unstart and low Mach number unstart phenomena) is referred to Refs 10, 16 and 21.

3.0 CLASSIFICATION OF HYPERSONIC INLET START/UNSTART BY USING PROBABILISTIC OUTPUT SVM

In this section, we firstly present the classification of hypersonic inlet start/unstart based on SVM, then discuss the necessaries of introducing the probabilistic output SVM to overcome or weaken the influence of the sensor noises on the classification accuracy of hypersonic inlet start/unstart. Finally the probabilistic output SVM is introduced and how to determine the membership function is given.

https://doi.org/10.1017/S0001924000002931 Published online by Cambridge University Press

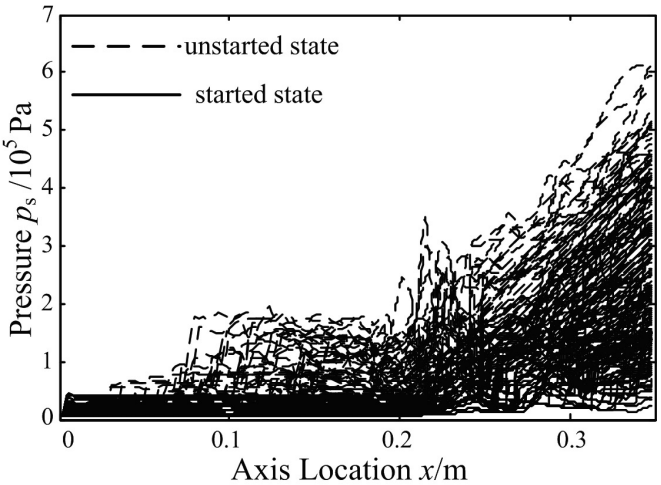

Figure 7. Surface pressure distributions with different boundary conditions.

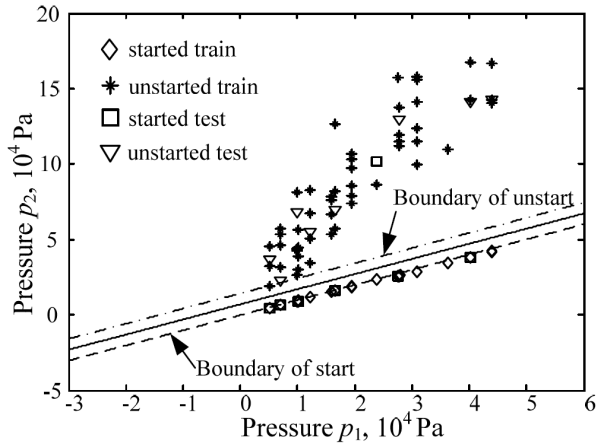

Figure 8. Train and test of hypersonic inlet start/unstart classification.

3.1 Pattern classification of hypersonic inlet start/unstart

Generally speaking, for the fixed-geometry inlet, the boundary between the inlet start and unstart is a very complex function of Mach number of freestream, angle of attack, pressure of freestream, and the pressure at the exit of isolator(or the fuel rate). Determining the boundary approximate function expression is difficult involving these variables, so the pattern classification of hypersonic inlet start/unstart is difficult. Three sets of boundary conditions identified in Table 1 were analysed as the representative operating conditions for a hypersonic inlet. The ramp surface pressure distributions of the inlet at different boundary conditions are shown in Fig. 7. It includes 117 different surface pressure distributions of inlet started and 62 distributions of inlet unstarted. The high dimension of data set brings great difficulty in understanding the data, constructing classifier for pattern classification. As can be seen from Fig. 7, there are no intuitively distinct features by which the inlet start/unstart could be classified. Therefore, it is necessary to introduce the knowledge of the feature selection and various intelligence algorithms to solve classification problems of inlet start/unstart.

Yu[16] discussed the feature selection,pattern classification,and optimal classification criterions of hypersonic inlet start/unstart without the sensor noises by using support vector machine. The two classes of feature attributions [3, 7, 11] and [80, 91, 99, 110, 122, 130] are found; here 3 denotes the third pressure point for every surface pressure distribution and so on. The axis location of every feature attribution is as follows: 3: 0·0039m, 7: 0·0117m, 11: 0·0200m, 80: 0·1546m, 91: 0·1761m, 99: 0·1851m, 110: 0·1884m, 122: 0·1919m, and 130: 0·1942m. Three groups of 18 combinations are achieved based on the two classes of feature attributions and are shown in Table 3. Here the 1-1 combination of [3, 80] is chosen as an example to illustrate the pattern classification of inlet start/unstart, and the classification is shown in Fig. 8. The classification hyperplane $p_2 - 1{\cdot}0033 \times p_1 - 6995{\cdot}3 = 0$ is obtained, here p_1 and p_2 are the pressure of 3rd and 80th respectively. There exist two boundaries, one is the boundary of inlet start, and the other is the boundary of inlet unstart. The classification criterions are described as follow. If $p_2 - 1{\cdot}0033 \times p_1 - 14{,}301 > 0$, the inlet is unstarted; else if $p_2 - 1{\cdot}0033 \times p_1 + 310{\cdot}4 < 0$, the inlet is started.

The physical significance of the classification criterions is explained in below. p_1 is located behind of the first oblique shock, and its magnitude depends on the intensity of shock, namely depends on M_∞, p_∞ and α, the magnitude of p_1 denotes the freestream conditions. If the freestream conditions are fixed, the inlet start/unstart can be determined by only p_2 for the fixed geometry inlet. When the inlet is unstart, the separated flow appears and the backward shock is formed, which results in an abrupt and large increase of p_2. However the freestream conditions are variational, and there exits that p_2 of inlet started at higher Mach number and positive angle of attack is greater than p_2 of inlet unstarted at lower Mach number and negative angle of attack. Thus determining the inlet weather start or unstart by only p_2 is not enough, p_1 which denotes the freestream conditions should be added.

3.2 Necessaries of introducing probabilistic output support vector machines

In ground and flight tests, it is inevitably to introduce the sensor noises and outer disturbances to the measurement system. The experimental study on the dynamics of supersonic/hypersonic inlet unstart[22-24] has been developed recently, and the variations of the pressure of inlet start and unstart with the time and frequency were given. Reference 23 shows that the fundamental frequency of the pressure sensor noise is about 20Hz, so we assume that the fundamental frequency of the pressure sensor noise used in this paper is 20Hz. The power of the pressure sensor noise can be varied by changing the magnitude. Figure 9 shows the classification of inlet start/unstart with the sensor noises. There exist some points appearing in the isolated belts due to the effect of the sensor noises, when the decision-making of engine control system is different from the inlet start and unstart, and the pattern of inlet start/unstart can be

Table 3
Different combinations of feature attributions

Group one, sequence number	1-1	1-2	1-3	1-4	1-5	1-6
Feature attributions	[3, 80]	[3,91]	[3,99]	[3,110]	[3,122]	[3,130]
Group two, sequence number	2-1	2-2	2-3	2-4	2-5	2-6
Feature attributions	[7, 80]	[7,91]	[7,99]	[7,110]	[7,122]	[7,130]
Group three, sequence number	3-1	3-2	3-3	3-4	3-5	3-6
Feature attributions	[11, 80]	[11,91]	[11,99]	[11,110]	[11,122]	[11,130]

https://doi.org/10.1017/S0001924000002931 Published online by Cambridge University Press

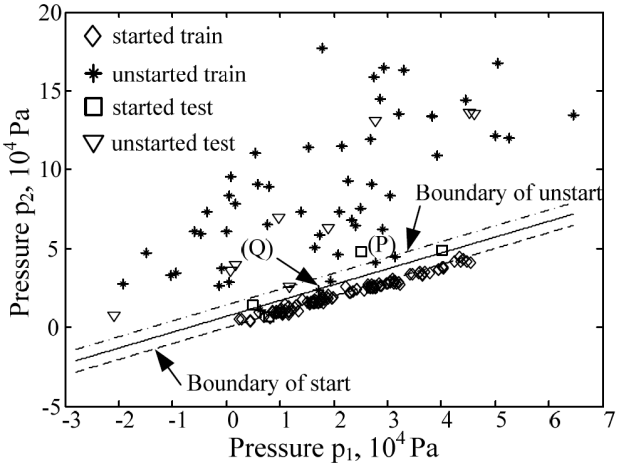

Figure 9. Train and test of hypersonic inlet start/unstart classification.

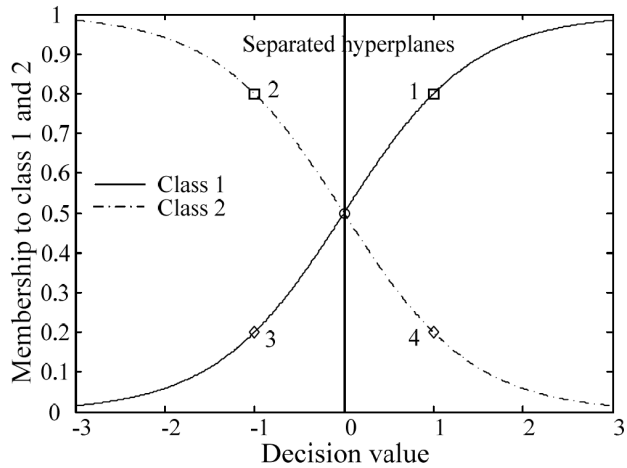

Figure 10. Variations of the membership with the decision value.

probably sensed falsely. Point *P* and *Q* (show in Fig. 9) should denote the inlet start and unstart, while they denote the inlet unstart and start respectively. Obviously, the detection of inlet start/unstart is falsely sensed. The classification accuracy of the hypersonic inlet start/unstart will be decreased due to the sensor noises and disturbances. The classification accuracy of the hypersonic inlet start/unstart is 100% without the sensor noise, while it is 79·14% with the sensor noise. The bigger the intensity of the noises and disturbances is, the lower the classification accuracy of the hypersonic inlet start/unstart is. So it is necessary to find more information by other intelligent algorithms, which will be helpful for the further decision and analysis.

3.3 Probabilistic output support vector machines

Fuzzy set theory has been introduced to support vector machines recently. Lin[25] developed the fuzzy memberships to evaluate the importance of data points to deal with this problem, and researchers paid much attention to automatically setting the fuzzy memberships of the training data points[25,26]. In a word, the fuzzy membership function is introduced to treat data points with different importance. A fuzzy output SVM[27], which not only gives the decision class of the data points, but also the location information in the feature space through the fuzzy membership. That is, we introduce the membership function to treat the decision with different importance.

Platt[28] provided a kernel method where a standard SVM plus sigmoid is trained to yield a posterior probability, which is presented as a probability output support vector machines. A sigmoid is fit to map standard SVM outputs to posterior probabilities, and its function expression is $1/(1 + e^{Af+B})$. Firstly we can obtain the class-conditional density $q(f|y)$ with the sensor noises, and the posterior density $q(y = 1|f)$ is obtained by the Bayesian estimation of $q(f|y)$. If and only if $A < 0$, the monotonicity of $1/(1 + e^{Af+B})$ is guaranteed. The parameters A and B are found by minimising the negative log likelihood of the training data, which is a cross-entropy error

$$\text{function} -\sum_i t_i \log(q_i) + (1-t_i)\log(1-q_i) \quad ,$$

where $q_i = 1/(1 + e^{Af+B})$, $t_i = (y_i + 1)/2$. The optimisation problem is a two parameters minimisation. In this paper, they are performed by using a model-trust minimisation algorithm for robustness, whose pseudo-code is shown in Ref. 28. The membership function to each class can be achieved finally. For example, the membership function to class 1 and class 2 is shown in Fig. 10. There are some illustrations about the membership shown in below.

1. The membership of data lying on the hyperplane to the two classes is 0·5 respectively.
2. Data point 1, 3 and 2, 4 are the supports vectors to class 1 and class 2 respectively. The membership of data point 1 and 3 to class 1 is q_1 and $1 - q_1$, and the membership of data point 2 and 4 to class 2 is q_2 and $1 - q_2$ respectively, where q_1 and q_2 are varied by the varieties of the sensor noises.
3. For a binary classification problem, if the membership of the sample to class 1 is more than 0·5, then this sample is belong to class 1; if the membership of the sample to class 1 is less than 0·5, then this sample is belong to class 2.
4. With the increase of the decision value, the membership to class 1 is towards 1; with the decrease of the decision value, the membership to class 2 is towards 1.

4.0 MULTIPLE CLASSIFIERS FUSION OF HYPERSONIC INLET START/UNSTART

Information fusion technology of multiple classifiers can surpass the capability limit of a single classifier. It can overcome the shortcomings of a single classifier and realise the knowledge integration among multiple classifiers to achieve the better performance. Especially, the information fusion of heterogeneous multiple classifiers can display their complementary advantages among different classifier models and can make the classification prediction more accurate and robust. Multiple classifiers combination has met significant success in many real-world recognition tasks in recent years[29], such as handwritten and text recognition[30], face recognition[31], time-series prediction[32]. There are many fusion algorithms such as majority voting[33], Bayesian classifier combination[30], boosting and bagging[34] and so on.

The fusion algorithm used in this paper is explained in below. The membership of the sample to hypersonic inlet start/unstart is computed by $\mu_i = 1/(1 + e^{Af_i+B})$ based on the probability output support vector machine, by which the membership matrix can be obtained in below.

$$\boldsymbol{\mu} = \begin{pmatrix} \mu_{11}\ \mu_{12} \cdots \mu_{1n} \\ \mu_{21}\ \mu_{22} \cdots \mu_{2n} \end{pmatrix}$$

Where μ_{1j} and μ_{2j} denote the membership of the start and unstart samples to inlet start by using the *j*th classifier respectively. The

https://doi.org/10.1017/S0001924000002931 Published online by Cambridge University Press

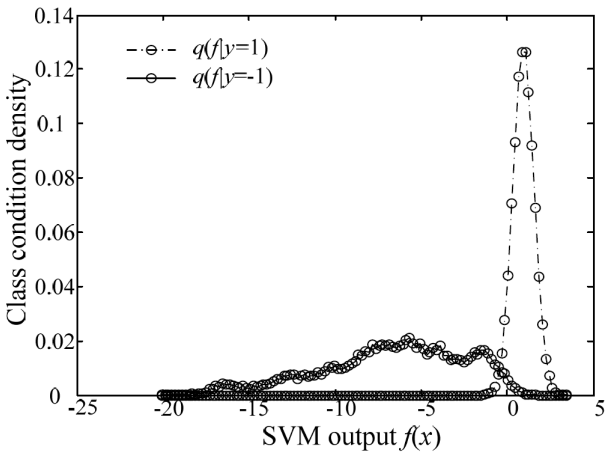

Figure 11. Class condition density of inlet start/unstart with the sensor noise.

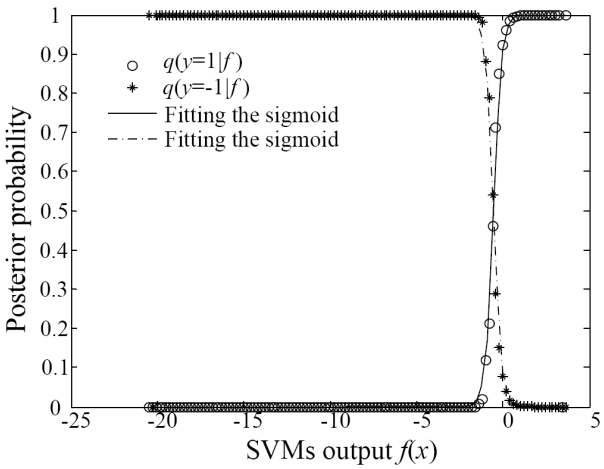

Figure 12. Posterior probabilities of inlet start/unstart with the sensor noise.

method used here is the mean fuzzy fusion, and the inlet start/unstart can be determined by

$$\bar{\mu}_i = (\sum_{j=1}^{n} \mu_{ij}(x)/n),\ i = 1,2$$

which satisfy $\bar{\mu}_1 + \bar{\mu}_2 = 1$. If $\bar{\mu}_1 \geq 0{\cdot}5$ this sample is classified to inlet start; if $\bar{\mu}_1 < 0{\cdot}5$, this sample is classified to inlet unstart. The algorithms of the multiple classifier fusion are described in below:

1. The characteristic of the pressure sensor noise are obtained firstly;
2. The membership functions of the different sensor noises are computed by the probabilistic output support vector machines;
3. The membership matrixes of every sample are obtained;
4. The decision value of every sample can be obtained by the comparison of $\bar{\mu}_1$ with 0·5.

We assume that the fundamental frequency of the pressure sensor noise used in this paper is 20Hz, and the power of the pressure sensor noise can be varied by changing the magnitude. The class conditional density of start/unstart are obtained and shown in Fig. 11, and the Bayesian estimation of which (the posterior density) is obtained and shown in Fig. 12, where $y = 1$ and $y = -1$ denote the samples belong to inlet start and inlet unstart respectively, f denotes the SVM output of the samples. The parameter A and B of the membership function $1/(1+e^{Af+B})$ can be obtained by the method in Section 3.3, and the variation of A and B with the intensity of the sensor noise is shown in Table 4. The effects of different pressure sensor noises on the classification accuracy of hypersonic inlet start/unstart were discussed in below.

Table 4
Variation of *A* and *B* with the intensity of the sensor noise

Power/dB	40	45	50	55	60	70
A	–13·07	–13·51	–13·38	–9·20	–4·25	–1·93
B	2·57	2·44	1·53	–0·75	–2·32	–2·55

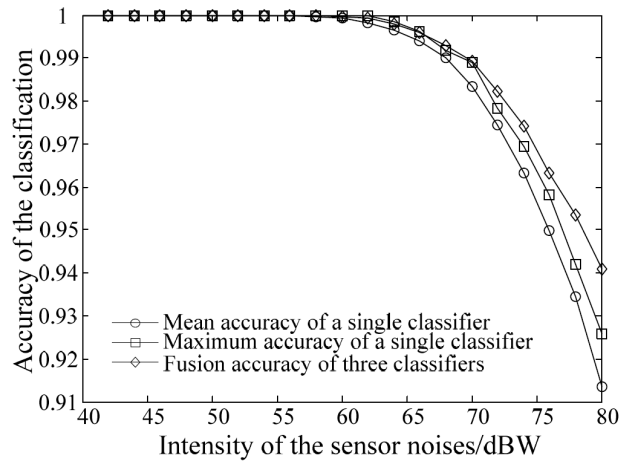

Figure13. Variations of the classification accuracy with the intensity of the sensor noises.

The accuracy of a classifier or several fusion classifiers is drawn by the ten cross-validation tests, which can represent the true classification accuracy of the samples in contrast with one test to some extents. The effects of the multiple classifiers fusion on the classification accuracy of hypersonic inlet start/unstart with the sensor noises or the disturbances were discussed in below. The following three groups of 'classification experiments' were conducted:

1. the variation of the classification accuracy with the intensity of the sensor noise;
2. the variation of the classification accuracy with the intensity of the sensor noise when a sensor is suddenly with a larger disturbance;
3. the variations of the classification accuracy with the number of the classifiers.

The accuracy of a single classifier and multiple classifier fusion were given and discussed respectively.

4.1 Variations of the classification accuracy with the intensity of the sensor noise

The number of the fusion classifiers can be arbitrariness, here the three classifiers [3, 80], [7,110] and [11,130] are selected to illustrate the variation of the classification accuracy with the intensity of the sensor noise, the same is in below. The variations of the mean and maximum accuracy of the classifier [3, 80], and the fusion accuracy of the three classifiers with the intensity of the sensor noises are shown in Fig. 13. The mean and maximum accuracy of a single

https://doi.org/10.1017/S0001924000002931 Published online by Cambridge University Press

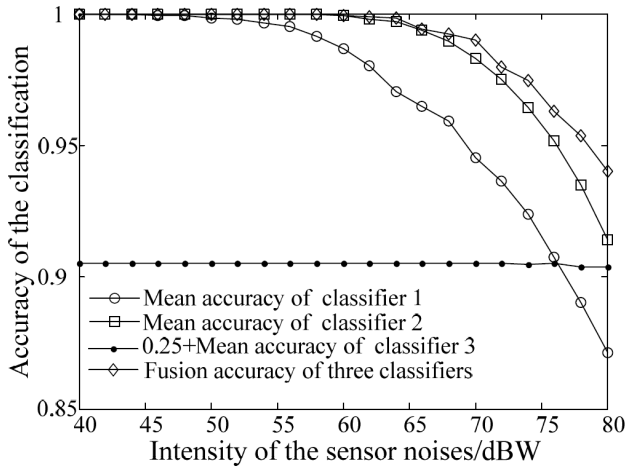

Figure 14. Variation of the classification accuracy with the intensity of the sensor noises.

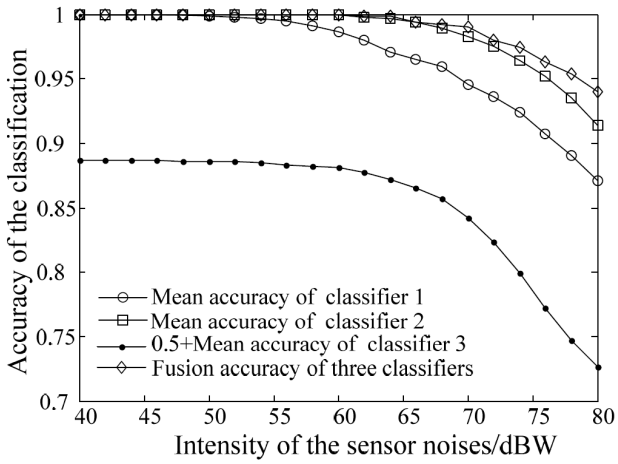

Figure 15. Variation of the classification accuracy with the intensity of the sensor noises.

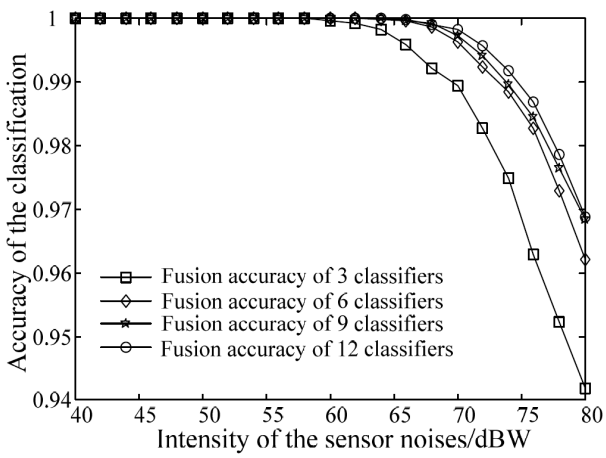

Figure 16. Variation of the classification accuracy with the intensity of the sensor noises.

classifier and the fusion accuracy of the three classifiers decrease with the increase of the intensity of the sensor noises. The fusion classification accuracy of three classifiers is bigger than the maximum classification accuracy of a single classifier. The more the intensity of the sensor noises is, the bigger the fusion classification accuracy of three classifiers is in contrast with a single classifier.

4.2 Variations of the classification accuracy with the intensity of the sensor noise when a sensor with a larger disturbance

The three classifiers [3, 80], [7,110] and [11,130] are also selected. The sensor characteristics probably encounter a larger disturbance besides the measurement noises. The larger disturbance is referred to that the senor is turned off or shorted. For the three classifiers, only a classifier can be assumed to be failure, otherwise the classification can not be detected truly using the three classifiers. The 110th sensor is assumed to be turned off and shorted, and the sensor characteristics are assigned to the maximum and minimum values respectively, and the variations of the mean classification accuracy of the classifier 1 [3, 80], the classifier 2 [11,130], the classifier 3 [7,110], and the fusion classification accuracy of the three classifiers with the intensity of the sensor noises are shown in Fig. 14 and Fig. 15 respectively. The classification accuracy of the classifier [7, 110] is very low due to the larger disturbance appearing in the 110th sensor, when it is necessary to combine the at least three classifiers to sense the inlet start or inlet unstart. The mean accuracy of a single classifier and the fusion accuracy of the three classifiers decrease with the increase of the intensity of the sensor noises. The fusion accuracy of three classifiers is bigger than the mean accuracy of a single classifier.

4.3 Variations of the classification accuracy with the number of the classifiers

The variations of the classification accuracy with the intensity of the sensor noises at different numbers of the classifier are shown in Fig. 16. With the increase of the number of the fusion classifiers, the fusion classification accuracy is improved at different intensity of the sensor noises. The larger the number of the fusion classifiers is, the bigger the fusion classification accuracy is. The larger number of the fusion classifiers means that the classification systems of inlet start/unstart is more complex, so there is a contradiction between the fusion classification accuracy and the number of the fusion classifiers. For example, when the number of the fusion classifier is from 9 to 12, the fusion classification accuracy is little increase. The number of the practical fusion classifiers needs a tradeoff between the fusion classification accuracy and the complexity of the classification system.

5.0 CONCLUSIONS

The investigation of the multiple classifiers fusion is motivated by the need for improving the reliability of the pattern classification of hypersonic inlet start/unstart. For this investigation, the POSVM algorithm and MCF methods are introduced to overcome or weaken the effect of the sensor noises and larger disturbances on the classification accuracy of hypersonic inlet start/unstart.

The category and membership function to hypersonic inlet start/unstart can be obtained by the POSVM algorithm, and the POSVM can give users the confidences of data points to inlet start/unstart. The effects of the MCF on the classification accuracy of hypersonic inlet start/unstart with the sensor noises or the disturbances are discussed. The variations of the classification accuracy with the intensity of the sensor noises are given. The result shows that using the technology of MCF can improve the classification

https://doi.org/10.1017/S0001924000002931 Published online by Cambridge University Press

accuracy of hypersonic inlet start/unstart with the sensor noises and outer disturbances. The larger the number of the fusion classifier is, the higher the fusion classification accuracy is, and the more complex the classification system is. The number of the practical fusion classifiers needs a tradeoff between the fusion classification accuracy and the complexity of the classification system.

ACKNOWLEDGEMENTS

This work was supported by China National Natural Science Foundation (No 90816028, No 90716012), and the authors thank the reviewer's valuable advices on this paper.

REFERENCES

1. CAMPBELL, D.H. F-12 series aircraft propulsion system performance and development, *J Aircr*, 1974, **11**, (11), pp 670-676.
2. SEDDON, J. and GOLDSMITH, E.L. *Intake Aerodynamics*, 1989, pp 149-168, AIAA Educational Series, AIAA, Washington DC.
3. MAYER, D. and PAYNTER, G.C. Prediction of supersonic inlet unstart caused by freestream disturbances, *AIAA J*, 1995, **33**, (2), pp 266-275.
4. MAYER, D. and PAYNTER, G.C. Boundary conditions for unsteady supersonic inlet analyses, *AIAA J*, 1994, **32**, (6), pp 1200-1206.
5. NEAVES, M.D., MCRAE, D.S. and EDWARDS, J.R. High-speed inlet unstart calculations using an implicit solution adaptive mesh algorithm, January 2001, AIAA Paper 2001-0825.
6. BENSON, R.A. and MCRAE, D.S. Numerical simulations of the unstart phenomenon in supersonic inlet/diffuser, June 1993, AIAA Paper 1993-2239.
7. ZHA, G.C., KNIGHT, D. and SMITH, D. Numerical investigations of high speed civil transport inlet unstart transient at angle of attack, *AIAA J Aircr*, 1998, **35**, (6), pp 851-856.
8. ZHA, G.C., KNIGHT, D. and SMITH, D. Numerical simulation of high speed civil transport inlet operability with angle of attack, *AIAA J Aircr*, 1998, **36**, (7), pp 1223-1229.
9. COX, C., LEWIS, C. and PAP. R. Prediction of unstart phenomena in hypersonic aircraft, April 1995, AIAA Paper 1995-6018.
10. CHANG, J., YU, D., BAO, W. and QU, L. Dimensionless analysis of the unstart boundary for 2D mixed hypersonic inlets, *Aeronaut J*, 2008, **112**, (1135), pp 547-555.
11. SCHMITZ, D.M. and BISSINGER, N.C. Design and testing of fixed geometry hypersonic intakes, April 1998, AIAA Paper 1998-1529.
12. VAN WIE, D.M. and KWOK, F.T. Starting characteristics of supersonic inlets, July 1996, AIAA Paper 1996-2914.
13. RREINARTZ, B.U. and HERRMANN, C.D. Aerodynamic performance analysis of a hypersonic inlet isolator using computation and experiment, *J Propul and Power*, 2003, **19**, (5), pp 868-875.
14. EMANI, S. and TREXLER, C.A. Experimental investigation of inlet combustor isolators for a dual-mode scramjet at a Mach number of 4, May 1995, NASA Technical Paper 3502.
15. HAWKINS, W. R. and MARQUART, E.J. Two-dimensional generic inlet unstart detection at Mach 2.5-5.0, April 1995, AIAA Paper 1995-6019.
16. YU, D., CHANG, J., BAO, W. and XIE, Z. Optimal classifications criterions of hypersonic inlet start/unstart, *J Propul and Power*, 2007, **23**, (2), pp 310-316.
17. VOLAND, R.T. and AUSLWNDER, A.H. CIAM/NASA Mach 6.5 scramjet flight and ground test, November 1999, AIAA Paper 1999-4848.
18. KULKARNI, S.R., LUGOSI, G. and VENKATESH, S.S. Learning pattern classification-a survey, IEEE Transactions on Information Theory, 1998, **44**, (6), pp 2178-2206.
19. DRIKAKIS, D. Advances in turbulent flow computations using high-resolution methods, *Progress in Aerospace Science*, 2003, **39**, pp 405-424.
20. HERRMANN,C.D. and KOSVHEL, W.W. Experimental investigation of the internal compression of a hypersonic intake, AIAA Paper 2002-4130.
21. CUI, T., YU, D., CHANG, J. and BAO, W. Topological geometry interpretation of hypersonic inlet start/unstart-catastrophe, hysteresis and bifurcation, *AIAA J Aircr*, 2008, **45**, (4), pp 1464-1468.
22. TRAPIER, S., DUVEAU, P. and DECK, S. Experimental study of supersonic inlet buzz, *AIAA J*, 2006, **44**, (10), pp 2354-2365.
23. TAN, H.J. and GUO, R.W. Experimental study of the unstable-unstarted condition of a hypersonic inlet at Mach 6, *J Propulsion and Power*, 2007, **23**, (4), pp 783-788.
24. WAGNER, J.L., VALDIVIA, A., YUCEIL, K.B., CLEMENS, N.T. and DOLLING, D.S. An experimental investigation of supersonic inlet unstart, 2007, AIAA Paper 2007-4352.
25. LIN, C. F. and WANG, S. D. Fuzzy support vector machines, 2002, IEEE Transaction on Neural Networks, **13**, (2,), pp 464-471.
26. HUANG, H.P. and LIU, Y.H. Fuzzy Support vector machines for pattern recognition and data mining, *Int J of Fuzzy Systems*, 2002, **4**, (3), pp 826-836.
27. XIE, Z.X., HU, Q,H. and YU, D.R. Fuzzy output support vector machines for classification, advances in natural computation, 2005, First International Conference, Changsha, China, August 2005, pp 1190-1197.
28. PLATT, J.C. Probabilistic outputs for support vector machines and comparisons to regularized likelihood methods, *Advances in Large Margin Classifiers*, 1999, MIT Press.
29. BATTITI, R. and COLLA, A. Democracy in neural nets: Voting schemes for classification, *Neural Networks*, 1994, **7**, (4), pp 691-707.
30. XU, L., KRZYZAK, A. and SUEN, C.Y. Method for combing multiple classifiers and their applications to handwriting recognition, *IEEE Transactions on Systems, Man, and Cybernetics*, 1992, **22**, (3), pp 418-435.
31. LV, X.G., WANG Y.H. and JAIN, A.K. Combining classifiers for face recognition, IEEE International Conference on Multimedia & Expo, July 2003, IEEE, Piscataway, NJ, pp 13-16.
32. DIETRICH, C., SCHWENKER, F. and PALM, G. Classification of time series utilizing temporal and decision fusion, February 2001, Proceedings of the Second International Workshop on Multiple Classifier Systems, Springer-Verlag, London, pp 378-387.
33. NADAL, C., LEGAULT, R. and SUEN, C.Y. Complementary algorithms for the recognition of totally unconstrained hand written numeral, June 1990, Proceedings of the 10th International Conference on Pattern Recognition, IEEE, Piscataway, NJ, pp 434-449.
34. SKURICHINA, M. and DUIN, R.P.W. Bagging, boosting and the random subspace method for linear classifiers, *Pattern Analysis & Applications*, 2002, **5**, (2), pp 121-135.